Chemistry
A European
Journal

Chemistry Europe
European Chemical Societies Publishing

Accepted Article

Title: Effect of Topology Structure on Photodynamic Sterilization of Porphyrinic Metal-Organic Frameworks

Authors: Yao-Yao Liu, Li-Jian Chen, Xu Zhao, and Xiu-Ping Yan

To be cited as: *Chem. Eur. J.* 10.1002/chem.202100920

Link to VoR: https://doi.org/10.1002/chem.202100920

WILEY-VCH

10.1002/chem.202100920

WILEY-VCH

Effect of Topology Structure on Photodynamic Sterilization of Porphyrinic Metal-Organic Frameworks

Yao-Yao Liu,[a,b] Li-Jian Chen,*[a,b] Xu Zhao,[a,b] and Xiu-Ping Yan*[a,b,c,d]

[a] Y.-Y. Liu, Dr. L.-J. Chen, Dr. X. Zhao, Prof. X.-P. Yan
State Key Laboratory of Food Science and Technology
Jiangnan University
Wuxi 214122, China
E-mail: chenlijian123@jiangnan.edu.cn
xpyan@jiangnan.edu.cn
[b] Y.-Y. Liu, Dr. L.-J. Chen, Dr. X. Zhao, Prof. X.-P. Yan
Institute of Analytical Food Safety
School of Food Science and Technology,Jiangnan University
Wuxi 214122, China
[c] Prof. X.-P. Yan
International Joint Laboratory on Food Safety
Jiangnan University
Wuxi 214122,China
[d] Prof. X.-P. Yan
Key Laboratory of Synthetic and Biological Colloids, Ministry of Education
Jiangnan University
Wuxi 214122, China

Supporting information and the ORCID identification number(s) for the author(s) of this article can be found under:

Abstract: Porphyrinic metal-organic frameworks (MOFs) are promising photosensitizers due to no self-aggregation of porphyrin in aqueous solution. However, how the topology of porphyrinic MOFs affects the generation of singlet oxygen ($^1O_2$) is unclear. Here, we report the effect of the topology of porphyrinic MOFs on their photodynamic performance. To this end, four porphyrinic zirconium MOFs (MOF-525, MOF-545, PCN-223 and PCN-224 with different topologies (**ftw**, **csq**, **shp** and **she** respectively)) were selected to study the influence of topology on the photodynamic antibacterial performance. The $^1O_2$ generation and the photodynamic antibacterial performance followed an decreasing order of MOF-545>MOF-525>PCN-224>PCN-223. The results reveal that the pore size, the distance between porphyrin and the number of porphyrin per Zr_6O_8 cluster in MOFs greatly affected the $^1O_2$ generation. This work provides a guidance for designing new MOFs for efficient photodynamic sterilization.

Introduction

Photodynamic sterilization combines the light of a specific wavelength, oxygen and photosensitizer to generate reactive oxygen species, especially singlet oxygen ($^1O_2$), for damaging microorganism unselectively via an oxidative burst.[1] So, it provides a broad spectrum of antibacterial property,[2] and few security issues.[3] The photosensitizer with excellent photosensitivity is the key for photodynamic sterilization. Traditional photosensitizers are mostly tetrapyrrole-containing compounds, such as chlorin, porphyrin and their derivatives. Porphyrin is a type of highly-conjugated macromolecular heterocyclic compound formed by the α-carbon atoms of four pyrrole subunits interconnected by a methine bridge (=CH-), and plays an important role in photodynamic sterilization.[4] However, the hydrophobicity of many porphyrins results in π-π stacking in aqueous solution, leading to self-quenching of porphyrins and reducing the production of $^1O_2$.[5] To avoid self-aggregation and self-quenching of porphyrins, porphyrinic metal-organic frameworks (MOFs) and other porphyrinic polymers are good alternative photosensitizers.[6]

MOFs, a kind of porous crystalline material, are assembled from metal ions or clusters and organic ligands.[7] MOFs are widely used in the fields of gas storage and separation,[8] adsorption,[9] biomedical application,[10] catalysis,[11] and sensing,[12] due to their high porosity, tunable structure and large surface area. Porphyrinic zirconium MOFs are an important subclass of MOFs,[13] assembled from porphyrin or metalloporphyrin as an organic bridging ligand and zirconium ion clusters as nodes through coordination bonds. The porphyrin units are periodically arranged in the frameworks to avoid self-quenching under the excited state,[14] and the porous structure of MOFs is beneficial to the diffusion of $^1O_2$.[15] Besides, the structure of porphyrinic zirconium MOFs are relatively stable, whether in water or acidic aqueous solution.[16] Porphyrinic zirconium MOFs are mainly used in photodynamic therapy of tumor,[6c,13e,17] photocatalysis,[13a,18] photodegradation of harmful substances.[19] Zhou's group synthesized size-controlled porphyrinic MOF (PCN-224) and used folic acid-functionalized PCN-224 for tumor-targeted photodynamic therapy.[13e] In recent years, porphyrinic zirconium MOFs were used for photodynamic sterilization.[2b,20] Jiang's group reported the PCN-224(Zr/Ti) with greatly enhanced antibacterial activity against multidrug-resistant pathogens under visible light for *in vivo* healing of the chronic wound infected by multidrug-resistant bacteria.[2b] Wang's group prepared MOF-525/poly(ε-caprolactone) mixed-matrix membrane as an effective photodynamic antibacterial agent against *Escherichia coli*.[20] Besides, the topology structure of porphyrinic zirconium MOFs was shown to influence their emissive property,[21] catalytic ability,[22] and gas storage.[23] The effect of different metal clusters on the $^1O_2$ generation of porphyrinic MOFs was also investigated.[24] However, the influence of MOFs' topology structure on the capacity of $^1O_2$ generation and photodynamic antibacterial ability has not been reported yet.

Herein, we report the effect of the topology of porphyrinic MOFs on their photodynamic performance. We choose four porphyrinic zirconium MOFs with different topology structures as models for this purpose. The four MOFs (MOF-525, MOF-545, PCN-223 and PCN-224) are based on the **ftw**, **csq**, **shp**, and **she** topologies, respectively, which are composed of Zr_6O_8 clusters connected by different numbers of meso-tetra(4-carboxyphenyl) porphyrin (TCPP).[13b] The ability of $^1O_2$ generation in water and the photodynamic antibacterial effects of the MOFs against *Escherichia coli* (*E. coli*) and *Staphylococcus aureus* (*S. aureus*) are compared, and the relationship between the topology structure and $^1O_2$ generation is discussed.

Results and Discussion

Characterization of four porphyrinic MOFs

The crystal structures of the synthesized porphyrinic MOFs were investigated by powder X-ray diffraction (PXRD) (Figure 1a-d). All sharp diffraction peaks match very well with the simulated patterns. The prepared MOF-525, MOF-545, PCN-223 and PCN-224 exhibited cubic (180 nm×180 nm), rod-shaped (260 nm×40 nm), spindle-shaped (230 nm×100 nm) and spherical (180 nm) morphology, respectively (Figure 1e-h, Figure S1-4). The elemental mass fraction of the MOFs by Energy-dispersive X-ray spectroscopy (EDS) and elemental mapping on a TEM was basically consistent with the theoretical composition of the MOFs, which proved the phase purity of the MOFs and the removal of guest molecules in the pores (Figure S5, Table S1). The absorption peaks of the MOFs were red-shifted and broadened compared with TCPP (Figure S6). The MOFs gave fluorescence emission peaks at 675 nm, 725 nm while TCPP exhibited fluorescence emission peaks at 650 nm, 725 nm (Figure S7). The above results are mainly caused by the periodic arrangement of TCPP in the different MOFs, which increases the electronic interaction between the TCPP units.[17a]

The porosity of MOFs was examined by nitrogen adsorption-desorption experiments at 77 K. MOF-525, MOF-545, PCN-223 and PCN-224 after activation gave the Brunauer-Emmett-Teller (BET) surface areas of 1687, 1079, 634 and 1789 m^2/g, respectively (Figure 2a-d). Nitrogen sorption isotherms of MOF-545 show a characteristic Type IV sorption profile (Figure 2b). Evaluation of a density functional theory (DFT) simulation from the nitrogen sorption curve revealed two types of pores (1.0 and 3.6 nm) (Figure 2b, inset), which are triangular microchannels and hexagonal meso-channels, respectively. Nitrogen sorption isotherms of MOF-525, PCN-223, PCN-224 show characteristic Type I sorption profiles (Figure 2a, c, d). The pore-size distribution analysis by using the DFT model revealed the different pore sizes of MOF-525 (2.0 nm), PCN-223 (1.1 nm), and PCN-224 (1.9 nm). The fitted curves in the pore size analysis were given in Figure S8-S11.

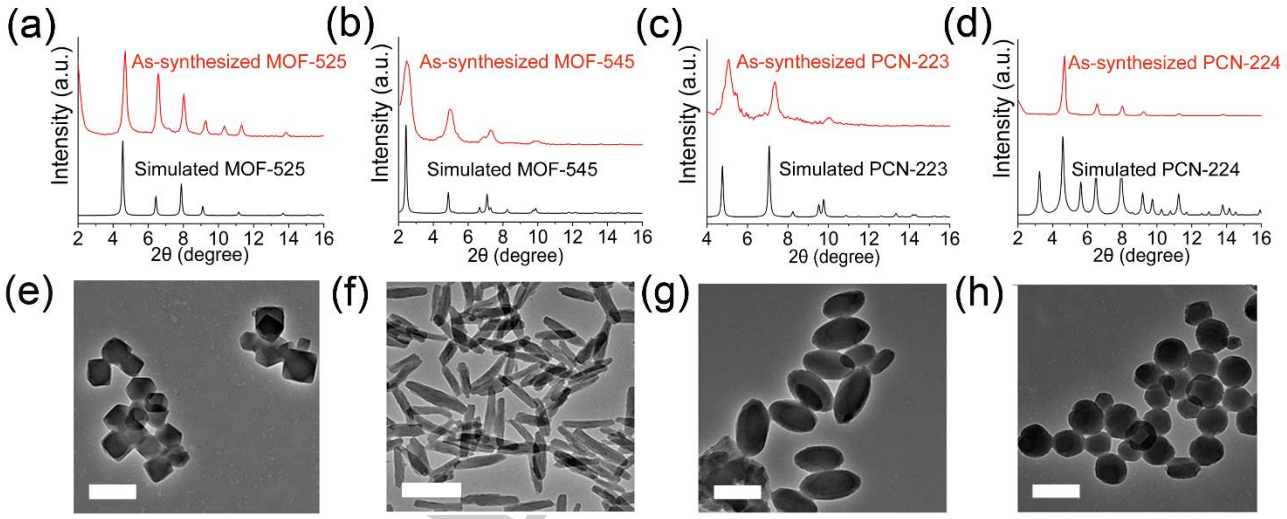

Figure 1. Experimental (red) and simulated (black) PXRD patterns: (a) MOF-525; (b) MOF-545; (c) PCN-223; (d) PCN-224. TEM images: (e) MOF-525; (f) MOF-545; (g) PCN-223; (h) PCN-224, scale bar: 200 nm.

Stability of MOFs in normal saline

The stability of porphyrinic zirconium MOFs in normal saline was investigated by inductively coupled plasma mass spectrometry (ICP-MS) and PXRD. No dissolved zirconium detected in the supernatant after immersing the MOFs in normal saline solution (0.9% NaCl) for 24 h by ICP-MS proved the stability of the MOFs in saline solution. Besides, the PXRD patterns of the four MOFs after soaking in saline for 24 h were consistent with those of the MOFs before soaking (Figure S12), which proved that no phase transition or framework collapse happened, also showing good stability of the MOFs in saline solution. Therefore, the porphyrinic zirconium MOFs are suitable for further photodynamic sterilization.

Comparison of $^1O_2$ generation of the MOFs and TCPP

The ability of MOFs and TCPP for $^1O_2$ generation in water was compared by the absorbance decrease of 9,10-anthracenediyl-bis(methylene) dimalonic acid (ABDA) under the irradiation of white LED light (4 mW/cm^2). ABDA can be oxidized by the generated $^1O_2$ to form peroxides, resulting in a decrease in the absorption of ABDA. The absorbance of ABDA in the presence of the MOFs decreased as irradiation time increased, whereas no apparent absorbance change occurred for ABDA alone or in the presence of TCPP (Figure S13-17), indicating only white

LED irradiation or its combination with TCPP did not affect the absorbance of ABDA. After irradiation for 40 min, the absorbance of ABDA decreased to 92% of the original absorbance in the presence of TCPP, revealing that little amount of $^1O_2$ generated of TCPP due to the self-aggregation of TCPP in water. However, the absorbance of ABDA decreased to 12%, 43%, 49%, 62% of the original absorbance in the presence of MOF-545, MOF-525, PCN-224 and PCN-223, respectively (Figure 2e). The above results reveal that the ability to generate $^1O_2$ followed an decreasing order of MOF-545>MOF-525>PCN-224>PCN-223.

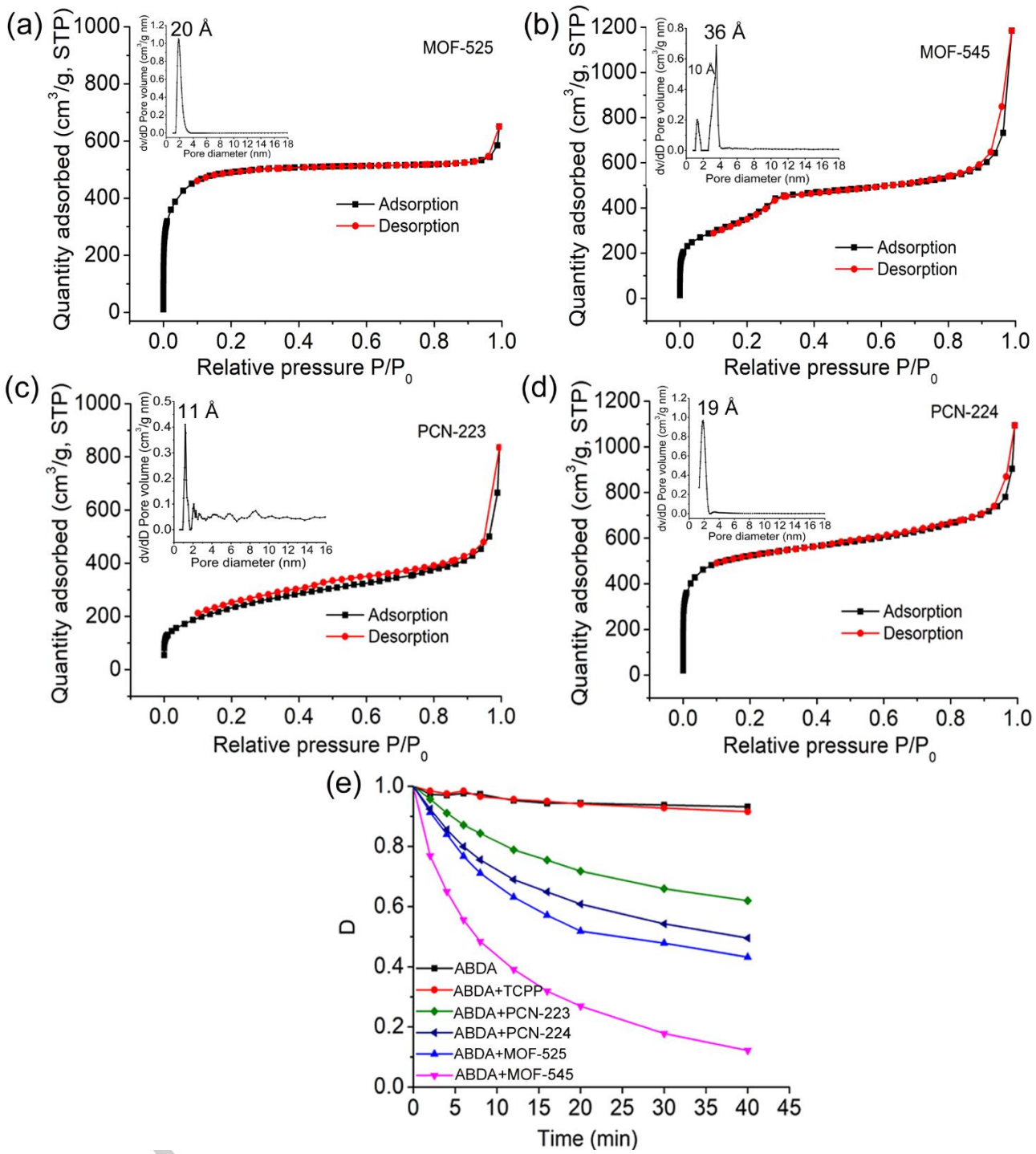

Figure 2. Nitrogen adsorption-desorption isotherms: (a) MOF-525; (b) MOF-545; (c) PCN-223; (d) PCN-224. The inset shows the corresponding pore size distribution. (e) Change of the absorbance of ABDA at 359 nm in the presence of the MOFs and TCPP with irradiation time by a white LED light. D = $(A–A_1)/(A_0-A_1)$, where A_0 was the initial absorbance of ABDA and MOF/TCPP, A was the absorbance of ABDA and MOF/TCPP at any irradiation time and A_1 was the absorbance of MOF/TCPP alone.

We then investigated the effect of the topology of the MOFs on the performance for $^1O_2$ generation. The topology structures of the four MOFs are illustrated in Figure 3a. These MOFs are composed of Zr_6O_8 clusters connected by different numbers of TCPP. The different topologies of the four MOFs result from the different kinds of coordination groups for Zr^{4+} ion, leading to different pore sizes and distances of the inter TCPP active sites.[11b] MOF-525 and PCN-224 have similar pore size distribution (20 Å for MOF-525 and 19 Å for PCN-224) and similar distance between inter TCPP active sites (13.7 Å for MOF-525 and 13.6 Å for PCN-224) in the frameworks, which leads to almost the same absorption spectra (Figure 3b). However, 12 TCPP molecules per Zr_6O_8 node in MOF-525 are two times those in PCN-224 (6 TCPP molecules per Zr_6O_8 node), resulting in better performance in $^1O_2$ generation. The result indicates the important role of the number of TCPP molecules per Zr_6O_8 node in $^1O_2$ generation.

The pore size and the distance between the TCPP active sites in the frameworks are another two important factors for $^1O_2$ generation. Although the number of TCPP molecules per Zr_6O_8 node in PCN-223 and MOF-525 is identical (both 12), MOF-525 has a larger pore size (20 Å) and a more far distance between the TCPP active sites (13.7 Å) than PCN-223 (11 Å and 10.7 Å for the pore size and the distance, respectively) in the frameworks (Figure 3a). The large pore size of MOF-525 is conducive to the diffusion of $^1O_2$ and more light penetration (Figure 3b) into the structure,[25] promoting the $^1O_2$ generation. MOF-545 and PCN-223 have similar triangular microchannel structures (pore size: 10 Å for MOF-545, 11 Å for PCN-223; distance between TCPP active sites: 10.9 Å for MOF-545, 10.7 Å for PCN-223), but MOF-545 has another hexagonal meso-channel structure, which features a larger distance between the TCPP active sites (18.3 Å) and pore size (36 Å) in the frameworks (Figure 3a). Although MOF-545 have fewer (8) TCPP molecules per Zr_6O_8 node than PCN-223 (12 TCPP molecules), the larger pore size and the longer distance of TCPP active sites may play a dominant role in promoting the light penetration (Figure 3b) and $^1O_2$ diffusion, leading to better performance for $^1O_2$ generation. In general, the $^1O_2$ production is dominated by the numbers of TCPP per Zr_6O_8 cluster in the MOFs with similar pore size and distance between TCPP active sites. However, the pore size and the distance of TCPP active sites will play a leading role in facilitating $^1O_2$ generation for the MOFs with the same or even the less number of TCPP per Zr_6O_8 cluster.

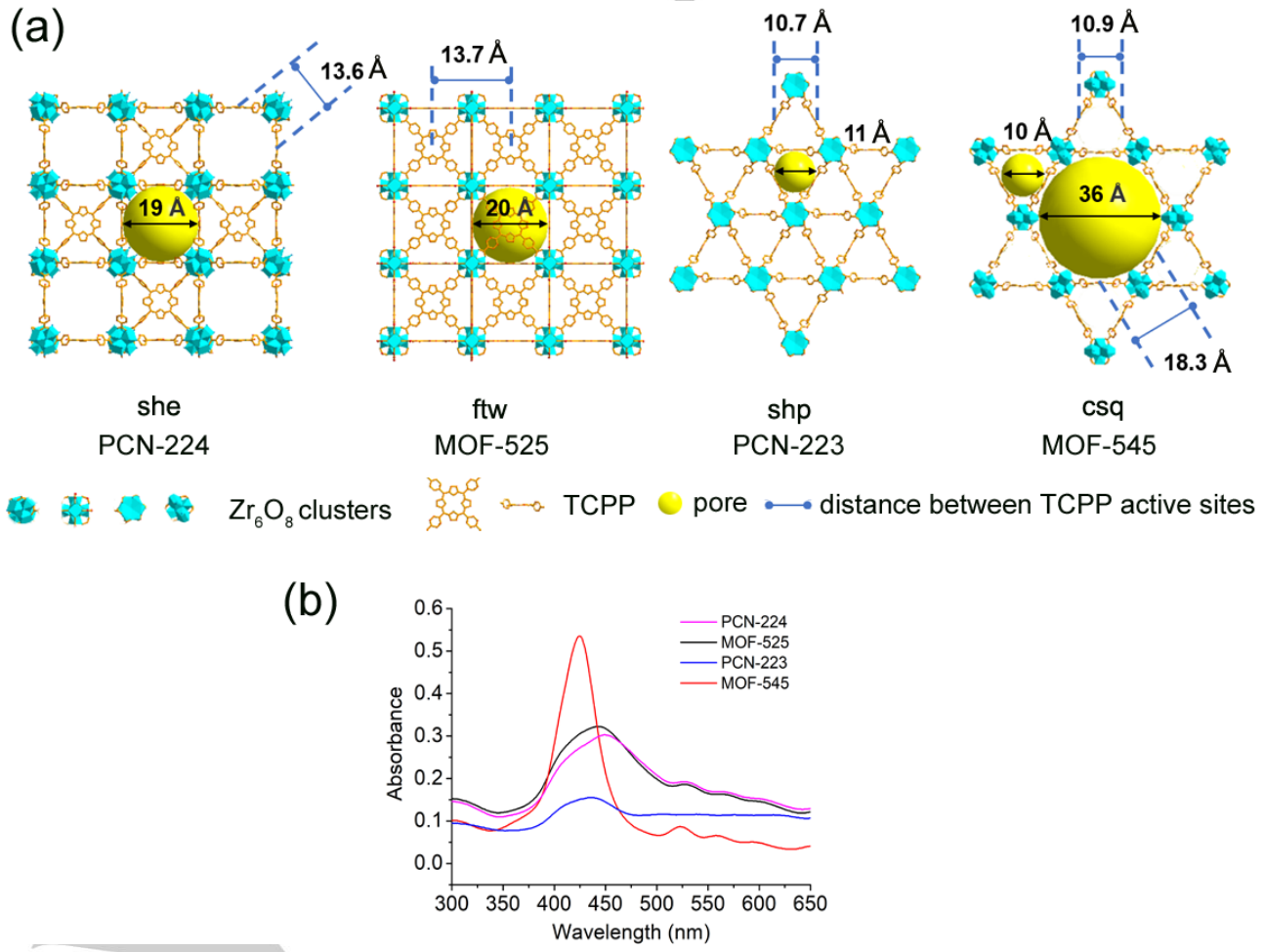

Figure 3. (a) Schematic topology structures of the four porphyrinic MOFs. (b) UV-vis absorption spectra of the MOFs in water (0.02 mg/mL).

$^1O_2$ production in *E. coli* and *S. aureus*

E. coli and *S. aureus* were chosen as representative gram-negative and gram-positive bacteria, respectively, to evaluate the photodynamic antibacterial performance of the MOFs *in vitro*. The $^1O_2$ generation in *E. coli* and *S. aureus* treated with various MOFs was detected by confocal laser scanning macroscopy (CLSM). 2,7-Dichlorodi-hydrofluorescein diacetate (DCFH-DA, 5 μmol/L) was used to stain the cells as the probe for $^1O_2$ as it emits green fluorescence in the presence of $^1O_2$ in cells. No green fluorescence was observed in both *E. coli* and *S. aureus* incubated with all the studied MOFs in dark, indicating no $^1O_2$ generated in bacteria in dark (Figure 4). In constrast, obvious green fluorescence was observed in both *E. coli* and *S. aureus* incubated with the MOFs after white LED irradiation. Comparison of the green fluorescence intensities in bacteria incubated with different MOFs after irradiation reveals an decreasing order of MOF-545>MOF-525>PCN-224>PCN-223 for $^1O_2$ generation in bacteria (Figure S18), which is in agreement with the results in water (Figure 2e).

Photodynamic antibacterial performance

To show the antibacterial ability of the four MOFs, scanning electron microscope (SEM) images were collected to investigate the morphological changes of *E. coli* and *S. aureus* after incubation with different MOFs under white LED irradiation (4 mW/cm^2) for 20 min. *E. coli* and *S. aureus* in the absence of the MOFs (blank group) remained intact rod-shaped and spherical, respectively, and the surfaces were smooth (Figure 5). The bacteria incubated with the MOFs in dark maintained good shape. However, the cell membranes of both *E. coli* and *S. aureus* were distorted and wrinkled after irradiation (Figure 5), and the bacteria incubated with MOF-545 showed the most obvious damage among the four MOFs, followed by MOF-525, PCN-224, PCN-223 (as shown with the red arrow in Figure 5). Therefore, the porphyrinic zirconium MOFs can effectively generate $^1O_2$ under the irradiation of white LED to oxidize the cell membranes of bacteria, causing cell membrane rupture and final cell death.

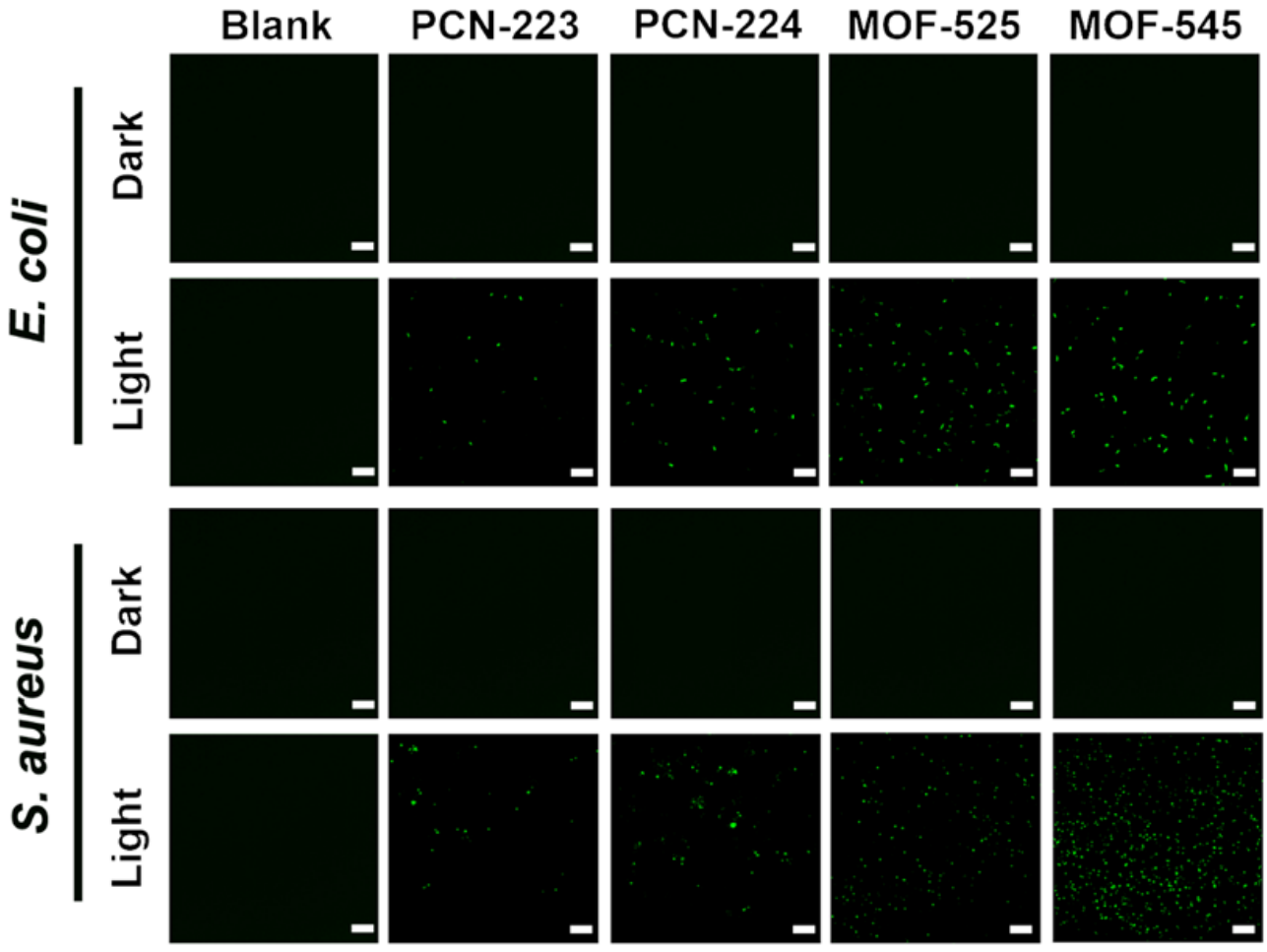

Figure 4. CLSM images of *E. coli* and *S. aureus* stained with DCFH-DA. Excitation: 488 nm; detection: 500-540 nm; scale bar: 2 μm. The bacteria were irradiated with a white LED light (4 mW/cm^2) or kept in dark for 20 min in the absence or presence of different MOFs (0.1 mg/mL)

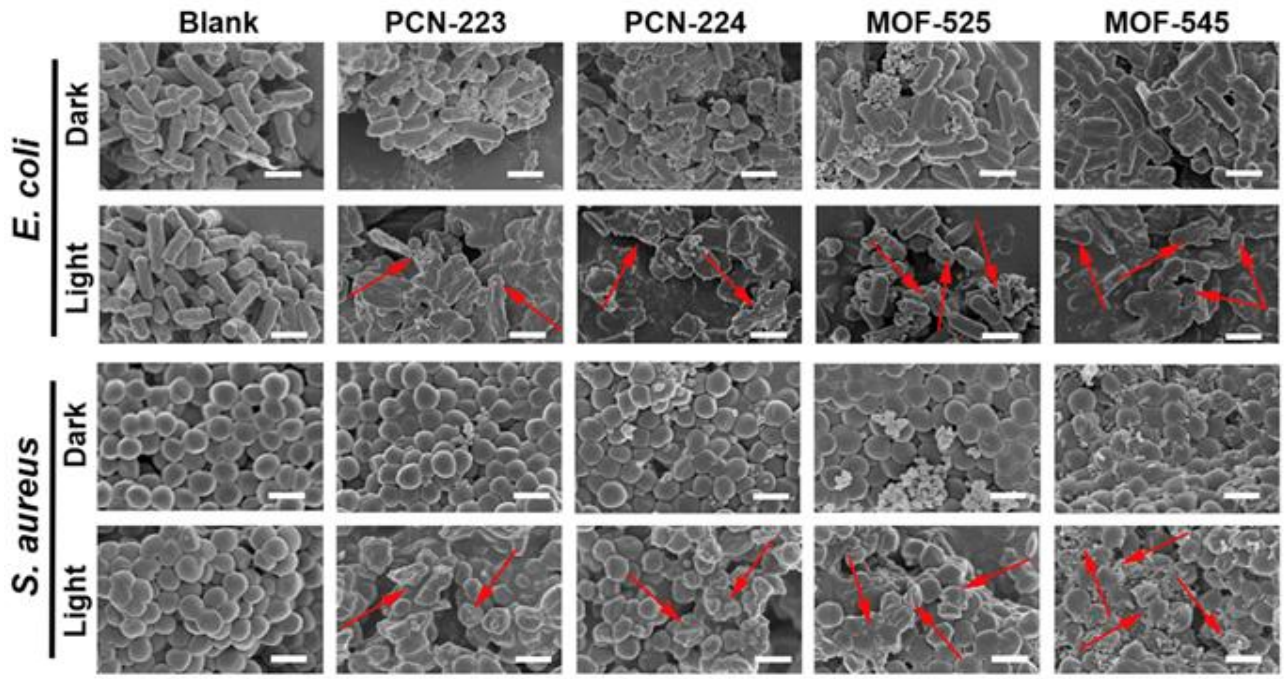

Figure 5. SEM images of *E. coli* (scale bar: 2 μm) and *S. aureus* (scale bar: 1 μm) irradiated (white LED light, 4 mW/cm^2) or kept in dark for 20 min in the absence or presence of different MOFs (0.1 mg/mL).

The viabilities and colony numbers of bacteria incubated with different concentrations of the four MOFs solution under 20 min-irradiation are shown in Figure 6 and 7. The bacterial viabilities for all the MOFs regardless of concentrations were almost the same as the blank group after being cocultured with *E. coli* or *S. aureus* for 20 min in dark, indicating that the MOFs have no or little antibacterial activity without light. In addition, there was no antibacterial effect of the MOFs under LED irradiation alone (Figure 6). The bacterial viability after irradiation decreased as the concentration of the MOFs increased (Figure 6). The bacterial colony pictures of *E. coli* and *S. aureus* incubated with different MOFs after irradiation are also shown in Figure 7. MOF-545, MOF-525, PCN-224 and PCN-223 (0.1 mg/mL) in combination with irradiation made the bacterial viability of *E. coli* decreased to 0.3%, 13.7%, 32.3%, 35.3%, respectively, and that of *S. aureus* reduced to 0.2%, 0.6%, 5%, 9.3%, respectively (Figure 6). The results show that the photodynamic antibacterial performance of the MOFs is similar to the ability for $^1O_2$ generation. The minimum bactericidal concentrations of MOF-545 against *E. coli* and *S. aureus* are 105 μg/mL and 100 μg/mL, respectively (Figure S19). The antibacterial performance of MOF-545 were also compared with that of other TCPP-containing materials against *E. coli* (Table S2). MOF-545 exposed to white LED light (4 mW/cm^2) for 20 min can reduce the number of *E. coli* colonies by 3 log while other TCPP-containing materials required higher power intensity or longer irradiation time.[6d,6f,26] In addition, The MOFs exhibited better photodynamic antibacterial performance for *S. aureus* than *E. coli* under the same experimental conditions due to the different cell wall structures of gram-negative and gram-positive bacteria.[5] *S. aureus* with porous layer of peptidoglycan and lipoteichoic acid is more susceptible to be damaged than *E. coli* with a many-layered outer surface.

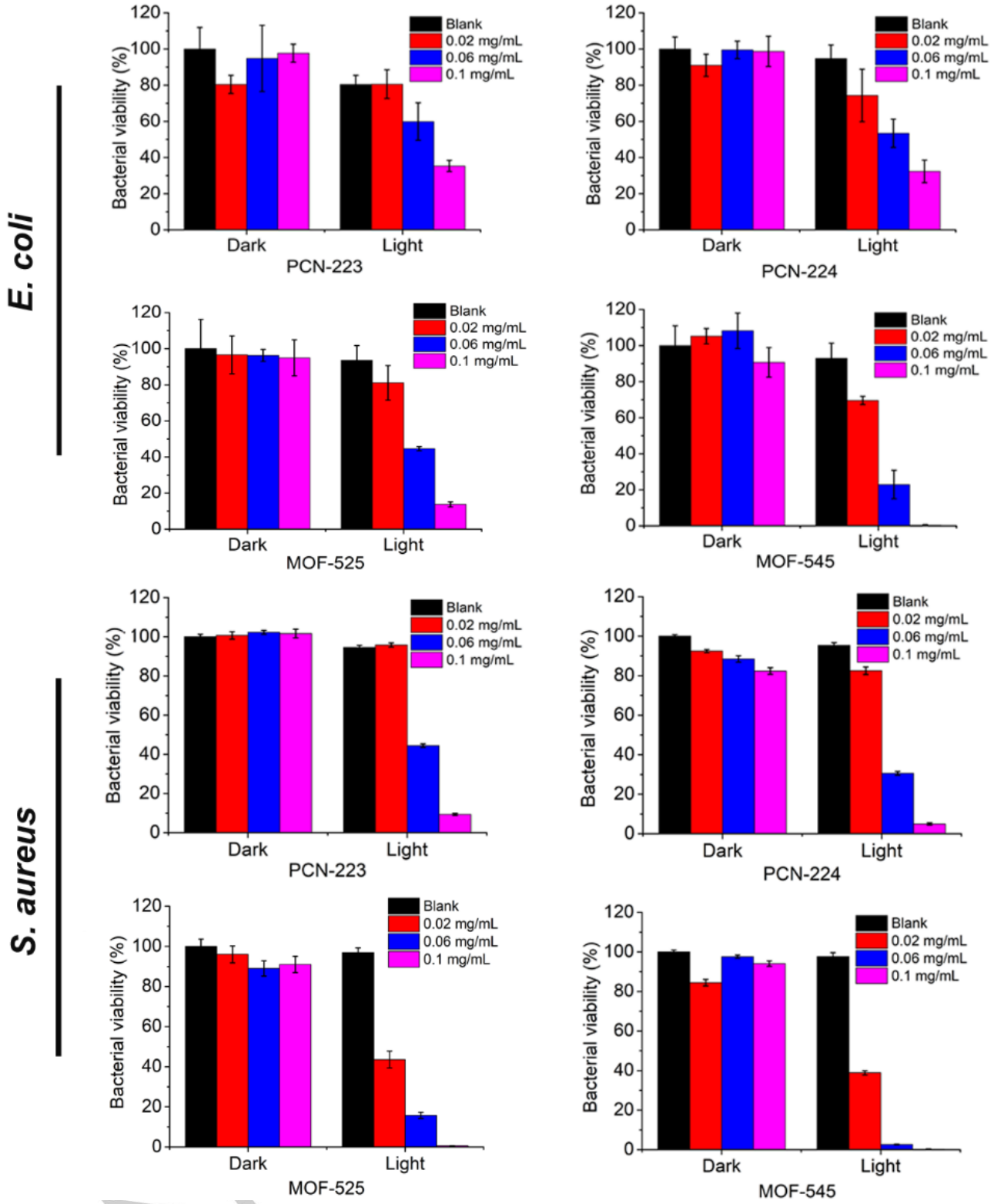

Figure 6. Bacterial viability of *E. coli* and *S. aureus* incubated with different concentrations of MOFs (blank, 0.02 mg/mL, 0.06 mg/mL, 0.1 mg/mL) under white LED light irradiation (4 mW/cm^2) or kept in dark for 20 min.

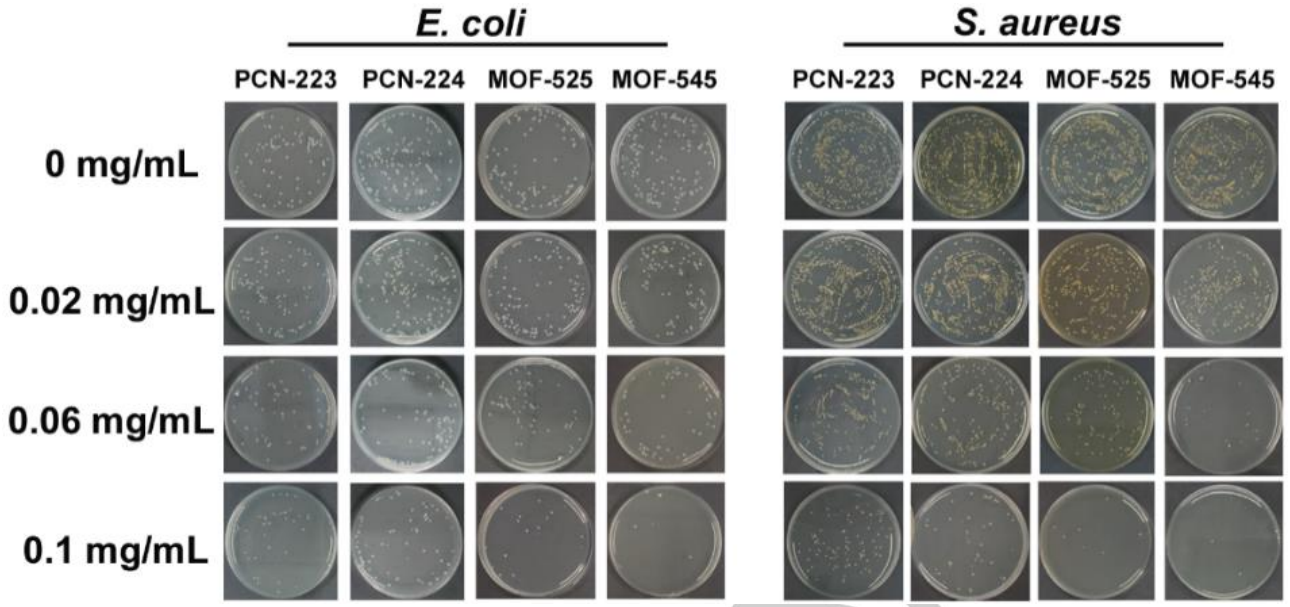

Figure 7. Photographs of the bacterial colonies of *E. coli* and *S. aureus* in the absence or presence of different MOFs under white LED light irradiation (4 mW/cm^2) for 20 min.

Conclusion

In summary, we have reported the effect of the topololgy structure of the porphyrinic zirconium MOFs on $^1O_2$ generation and photodynamic antibacterial performance. The variation in topology of the four MOFs due to different coordination groups for the Zr^{4+} leads to different pore sizes and different distances between inter TCPP active sites. The number of TCPP molecules per Zr_6O_8 cluster, the pore size and the distance between inter TCPP active sites play important roles in $^1O_2$ production. For the MOFs with similar pore size and distance between TCPP active sites, $^1O_2$ production is dominated by the numbers of TCPP molecules per Zr_6O_8 cluster in the frameworks, while for the MOFs with the same or even less number of TCPP molecules per Zr_6O_8 cluster the pore size and the distance between TCPP active sites play a leading role in facilitating $^1O_2$ generation. Porphyrinic zirconium MOFs with large pore size, long distance between inter TCPP active sites as well as large number of TCPP molecules per Zr_6O_8 cluster in the frameworks are good candidates as photosentisizers for photodynamic sterilization. This work provides a good guidance for the design of new MOFs as photosensitizers in photodynamic sterilization and therapy.

Experimental Section

Preparation of the MOFs

MOF-525, MOF-545, PCN-223 and PCN-224 were prepared according to Kelty et al.,[13c] Bůžek et al.,[17b] Feng et al.,[13d] and Park et al.,[13e] respectively.

Evaluation of $^1O_2$ Generation

The solution of ABDA in DMSO (15 μL, 5 mmol/L), aqueous MOF dispersion (30 μL, 1 mg/mL) or TCPP solution (15 μL, 1.3 mg/mL) were added into a 2-mL transparent centrifuge tube. The mixture solution was made to 1.5 mL with ultrapure water, then mixed thoroughly. The blank solution was prepared in parallel without addition of the MOFs or TCPP. The solutions were irradiated by the white LED light (4 mW/cm^2) for 0, 2, 4, 6, 8, 12, 16, 20, 30 and 40 min, and the UV-vis absorption spectra were recorded on a UV-vis-NIR spectrophotometer. The absorbance of MOFs or TCPP at 359 nm was subtracted for the reason that both MOFs/TCPP and ABDA have absorbance at 359 nm When calculating the changes of the absorbance of ABDA.

Stability Test for the MOFs in 0.9% Saline

Various amounts of the MOFs were dispersed in 0.9% saline. After 24 h, the supernatants were collected by centrifugation (10000 rpm, 20 min) for the ICP-MS determination of zirconium. The PXRD patterns of the MOFs precipitation after drying under vaccum were tested.

Preparation of bacterial cultures

The original *E. coli* or *S. aureus* suspension (10 μL) was cultured in 5 mL Luria Bertani (LB) broth medium with shaking (180 rpm) at 37°C for 12 h. Bacteria harvesting was done at mid-log phase by centrifuging at 4000 rpm for 7 min, then resuspended in LB broth medium to the concentration of 10^7 colony forming units (CFU)/mL.

Detection of $^1O_2$ in *E. coli* and *S. aureus*

The bacterial suspension (850 μL, 10^7 CFU/mL) was mixed with DCFH-DA (50 μL, 100 μmol/L), then the mixture was incubated with MOF dispersion (100 μL, 1 mg/mL) at 37°C for 2 h in dark. Bacteria suspension without MOFs was set as the blank group. After dark or light treatment for 20 min, the hybrid of bacteria was centrifuged (4000 rpm,10 min), and washed with 0.9% saline for two times, then resuspended in 0.9% saline. Bacterial solution (10 μL) was dropped onto a glass slide which was treated with poly-L-lysine previously. Fluorescent images were collected on CLSM.

Observation of bacterial morphology

The bacteria suspensions (900 μL, 10^7 CFU/mL) were incubated with 100 μL of 0.9% saline or MOF dispersion at 37°C in dark for 2 h. Then, experimental group was treated under white LED light (4 mW/cm^2) irradiation for 20 min while the control group was kept in dark. The hybrid of bacteria was centrifuged (4000 rpm,10 min) and washed with 0.9% saline for two times. Then, the hybrid of bacteria was fixed in 2.5% glutaraldehyde for 16 h. Finally, the bacteria were dehydrated gradiently in ethanol solution with different concentrations (30%, 50%, 70%, 80%, 95% and 100% v/v) for 10 min. After the bacteria were dried and gold was sprayed, SEM images were collected.

Evaluation of photodynamic antibacterial performance

The bacterial suspensions (500 μL, 10^7 CFU/mL) were mixed with different volumes of MOF dispersion (0, 20, 60, 100 μL, respectively; 1 mg/mL), then incubated with different volumes of LB broth medium at 37°C for 2 h to make the MOF's final concentrations of 0, 0.02, 0.06 and 0.1 mg/mL, respectively. In the experimental group, the solution was irradiated with a LED white light (4 mW/cm^2) for 20 min, while the control group was kept in dark. Finally, each group was serially diluted with 0.9% saline. The final dilutions (100 μL) were spotted onto LB agar plates and incubated at 37°C overnight. The colonies numbers were counted on the LB plate.

Acknowledgements

The authors are thankful for the financial support from National Natural Science Foundation of China (No. 21934002, 21804057, and 21804056), and Natural Science Foundation of Jiangsu Province, China (No. BK20180584 and BK20180581), and Collaborative Innovation Center of Food Safety and Quality Control in Jiangsu Province.

Keywords: porphyrinic zirconium metal-organic frameworks • singlet oxygen generation • photodynamic sterilization

[1] a) F. Cieplik, D. Deng, W. Crielaard, W. Buchalla, E. Hellwig, A. Al-Ahmad, T. Maisch, *Crit. Rev. Microbiol.* **2018,** *44,* 571-589; b) T. Kikuchi, M. Mogi, I. Okabe, K. Okada, H. Goto, Y. Sasaki, T. Fujimura, M. Fukuda, A. Mitani, *Int. J. Mol. Sci.* **2015,** *16,* 24111-24126.

[2] a) M. R. Hamblin, *Curr. Opin. Microbiol.* **2016,** *33,* 67-73; b) M. Chen, Z. Long, R. Dong, L. Wang, J. Zhang, S. Li, X. Zhao, X. Hou, H. Shao, X. Jiang, *Small* **2020,** *16,* 1906240.

[3] W. C. de Melo, P. Avci, M. N. de Oliveira, A. Gupta, D. Vecchio, M. Sadasivam, R. Chandran, Y. Y. Huang, R. Yin, L. R. Perussi, G. P. Tegos, J. R. Perussi, T. Dai, M. R. Hamblin, *Expert Rev. Anti-Infect. Ther.* **2013,** *11,* 669-693.

[4] M. Lismont, L. Dreesen, S. Wuttke, *Adv. Funct. Mater.* **2017,** *27,* 1606314.

[5] B. M. Amos-Tautua, S. P. Songca, O. S. Oluwafemi, *Molecules* **2019,** *24*, 2456.

[6] a) J. Hynek, J. Rathouský, J. Demel, K. Lang, *RSC Adv.* **2016,** *6,* 44279-44287; b) E. Káfuňková, K. Lang, P. Kubát, M. Klementová, J. Mosinger, M. Šlouf, A.-L. Troutier-Thuilliez, F. Leroux, V. Verney, C. Taviot-Guého, *J. Mater. Chem.* **2010,** *20,* 9423-9432; c) L. Zhang, J. Lei, F. Ma, P. Ling, J. Liu, H. Ju, *Chem. Commun.* **2015,** *51,* 10831-10834; d) J. Li, W. Sun, Z. Yang, G. Gao, H. H. Ran, K. F. Xu, Q. Y. Duan, X. Liu, F. G. Wu, *ACS Appl. Mater. Interfaces* **2020,** *12*, 54378-54386; e) R. Khan, M. Ozkan, A. Khaligh, D. Tuncel, *Photochem. Photobiol. Sci.* **2019,** *18,* 1147-1155; f)Y. Zhang, J. Ma, D. Wang, C. Xu, S. Sheng, J. Cheng, C. Bao, Y. Li, H. Tian, *Biomater. Sci.* **2020,** *8,* 6526-6532.

[7] a) S. Yuan, L. Feng, K. Wang, J. Pang, M. Bosch, C. Lollar, Y. Sun, J. Qin, X. Yang, P. Zhang, Q. Wang, L. Zou, Y. Zhang, L. Zhang, Y. Fang, J. Li, H. C. Zhou, *Adv. Mater.* **2018,** *30,* 1704303; b) A. Schneemann, V. Bon, I. Schwedler, I. Senkovska, S. Kaskel, R. A. Fischer, *Chem. Soc. Rev.* **2014,** *43,* 6062-6096; c) Z. Chang, D. H. Yang, J. Xu, T. L. Hu, X. H. Bu, *Adv. Mater.* **2015,** *27,* 5432-5441.

[8] C. Janiak, *Chem. Commun.* **2013,** *49,* 6933-6937.

[9] Q. Gao, J. Xu, X.-H. Bu, *Coord. Chem. Rev.* **2019,** *378,* 17-31.

[10] P. Horcajada, R. Gref, T. Baati, P. K. Allan, G. Maurin, P. Couvreur, G. Férey, R. E. Morris, C. Serre, *Chem. Rev.* **2011,** *112,* 1232-1268.

[11] a) R. K. Das, A. Aijaz, M. K. Sharma, P. Lama, P. K. Bharadwaj, *Chemistry* **2012,** *18,* 6866-6872; b) X. Gong, Y. Shu, Z. Jiang, L. Lu, X. Xu, C. Wang, H. Deng, *Angew. Chem. Int. Ed.* **2020,** *59,* 5326-5331; *Angew. Chem.* **2020,** *132,* 5364 –5369.

[12] Y. Takashima, V. M. Martinez, S. Furukawa, M. Kondo, S. Shimomura, H. Uehara, M. Nakahama, K. Sugimoto, S. Kitagawa, *Nat. Commun.* **2011,** *2,* 168.

[13] a) D. Feng, Z. Y. Gu, J. R. Li, H. L. Jiang, Z. Wei, H. C. Zhou, *Angew. Chem. Int. Ed.* **2012,** *51,* 10307-10310; *Angew. Chem.* **2012,** *124,* 10453 –10456; b) W. Morris, B. Volosskiy, S. Demir, F. Gandara, P. L. McGrier, H. Furukawa, D. Cascio, J. F. Stoddart, O. M. Yaghi, *Inorg. Chem.* **2012,** *51,* 6443-6445; c) M. L. Kelty, W. Morris, A. T. Gallagher, J. S. Anderson, K. A. Brown, C. A. Mirkin, T. D. Harris, *Chem. Commun.* **2016,** *52,* 7854-7857; d) D. Feng, Z. Y. Gu, Y. P. Chen, J. Park, Z. Wei, Y. Sun, M. Bosch, S. Yuan, H. C. Zhou, *J. Am. Chem. Soc.* **2014,** *136,* 17714-17717; e) J. Park, Q. Jiang, D. Feng, L. Mao, H. C. Zhou, *J. Am. Chem. Soc.* **2016,** *138,* 3518-3525.

[14] T. Zhang, W. Lin, *Chem. Soc. Rev.* **2014,** *43,* 5982-5993.

[15] K. Lu, C. He, W. Lin, *J. Am. Chem. Soc.* **2014,** *136,* 16712-16715.

[16] Y. Bai, Y. Dou, L. H. Xie, W. Rutledge, J. R. Li, H. C. Zhou, *Chem. Soc. Rev.* **2016,** *45,* 2327-2367.

[17] a) X. Zhao, Z. Zhang, X. Cai, B. Ding, C. Sun, G. Liu, C. Hu, S. Shao, M. Pang, *ACS Appl. Mater. Interfaces* **2019,** *11,* 7884-7892; b) D. Bůžek, J. Zelenka, P. Ulbrich, T. Ruml, I. Křížová, J. Lang, P. Kubát, J. Demel, K. Kirakci, K. Lang, *J. Mater. Chem. B* **2017,** *5,* 1815-1821; c) G. Lan, K. Ni, W. Lin, *Coord. Chem. Rev.* **2019,** *379,* 65-81; d) K. Zhang, X. Meng, Y. Cao, Z. Yang, H. Dong, Y. Zhang, H. Lu, Z. Shi, X. Zhang, *Adv. Funct. Mater.* **2018,** *28,* 1804634.

[18] a) A. N. Meng, L. X. Chaihu, H. H. Chen, Z. Y. Gu, *Sci. Rep.* **2017,** *7,* 6297; b) C. Xu, H. Liu, D. Li, J. H. Su, H. L. Jiang, *Chem. Sci.* **2018,** *9,* 3152-3158; c) H. Q. Xu, J. Hu, D. Wang, Z. Li, Q. Zhang, Y. Luo, S. H. Yu, H. L. Jiang, *J. Am. Chem. Soc.* **2015,** *137,* 13440-13443.

[19] a) C. T. Buru, M. B. Majewski, A. J. Howarth, R. H. Lavroff, C. W. Kung, A. W. Peters, S. Goswami, O. K. Farha, *ACS Appl. Mater. Interfaces* **2018,** *10,* 23802-23806; b) W. Q. Zhang, K. Cheng, H. Zhang, Q. Y. Li, Z. Ma, Z. Wang, J. Sheng, Y. Li, X. Zhao, X. J. Wang, *Inorg. Chem.* **2018,** *57,* 4230-4233.

[20] M. Liu, L. Wang, X. Zheng, Z. Xie, *ACS Appl. Mater. Interfaces* **2017,** *9,* 41512-41520.

[21] P. Deria, J. Yu, R. P. Balaraman, J. Mashni, S. N. White, *Chem. Commun.* **2016,** *52,* 13031-13034.

[22] P. Deria, D. A. Gomez-Gualdron, I. Hod, R. Q. Snurr, J. T. Hupp, O. K. Farha, *J. Am. Chem. Soc.* **2016,** *138,* 14449-14457.

[23] D. A. Gomez-Gualdron, O. V. Gutov, V. Krungleviciute, B. Borah, J. E. Mondloch, J. T. Hupp, T. Yildirim, O. K. Farha, R. Q. Snurr, *Chem. Mat.* **2014,** *26,* 5632-5639.

[24] Q. Liu, H. Cong, H. Deng, *J. Am. Chem. Soc.* **2016,** *138*, 13822-13825.

[25] Y. Ding, Y. P. Chen, X. Zhang, L. Chen, Z. Dong, H. L. Jiang, H. Xu, H. C. Zhou, *J. Am. Chem. Soc.* **2017,** *139,* 9136-9139.

[26] a) M. Managa, E. K. Amuhaya, T. Nyokong, *Spectroc. Acta Pt. A-Molec. Biomolec. Spectr.* **2015,** *151,* 867-874; b) A. C. Scanone, N. S. Gsponer, M. G. Alvarez, E. N. Durantini, *J. Photochem. Photobiol. A-Chem.* **2017,** *346,* 452-461.

10.1002/chem.202100920

Entry for the Table of Contents

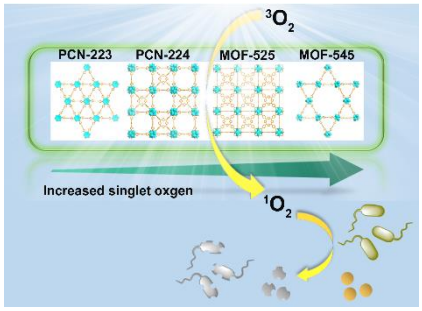

The effect of the topololgy structure of the porphyrinic zirconium MOFs on $^1O_2$ generation and photodynamic antibacterial performance was studied by taking MOF-545, MOF-525, PCN-224 and PCN-223 as model MOFs. The number of TCPP molecules per Zr_6O_8 cluster, the pore size and the distance between inter TCPP active sites which caused by the variation in topology of the MOFs play important roles in $^1O_2$ generation.